International Journal of Thermophysics (2025) 46:41
https://doi.org/10.1007/s10765-025-03512-w

Thermophysical Properties of $NbAlO_4$ and $TaAlO_4$

Julian Gebauer[1] · Magnus Rohde[1] · Peter Franke[1] · Hans Jürgen Seifert[1]

Received: 3 December 2024 / Accepted: 20 January 2025 / Published online: 8 February 2025

Abstract
Thermophysical properties of the ternary oxides $NbAlO_4$ and $TaAlO_4$ are experimentally determined. For $NbAlO_4$, the molar heat capacity is 98.9 J $(mol \cdot K)^{-1}$ at 0 °C up to 155.6 J $(mol \cdot K)^{-1}$ at 950 °C and for $TaAlO_4$ 97.1 J $(mol \cdot K)^{-1}$ at 0 °C up to 154.2 J $(mol \cdot K)^{-1}$ at 950 °C, respectively. Maier-Kelley polynomials are provided for the molar heat capacities. Thermal diffusivities in the range from 20 °C to 700 °C (α_{NbAlO_4}: from 0.009 to 0.004 $cm^2 \cdot s^{-1}$ and α_{TaAlO_4}: from 0.017 to 0.005 $cm^2 \cdot s^{-1}$), bulk densities at 25 °C (ρ_{NbAlO_4}= 3.94 $g \cdot cm^{-3}$ and ρ_{TaAlO_4}= 6.07 $g \cdot cm^{-3}$) and melting points of the oxides are measured, and the thermal conductivities are calculated from these properties. The thermal conductivity from 20 °C to 700 °C of $NbAlO_4$ λ_{NbAlO_4} is in the range from 0.020 to 0.013 $W \cdot cm^{-1} \cdot K^{-1}$ and of $TaAlO_4$ λ_{TaAlO_4} in the range from 0.039 to 0.015 $W \cdot cm^{-1} \cdot K^{-1}$, respectively. A porosity correction for thermal conductivities is applied, and with that, data for perfectly dense material are provided.

Keywords Calorimetry · Refractories · Specific heat capacity · Thermal conductivity

1 Introduction

The mixed oxides niobium aluminate $NbAlO_4$ and tantalum aluminate $TaAlO_4$ are of interest for new thermal barrier coatings (TBCs) and environmental barrier coatings (EBCs) [1]. Both have similar thermal expansion coefficients ($3.0–5.7 \cdot 10^{-6}$ K^{-1} at 100 °C to 1200 °C [1]) as SiC ceramics ($3.2–5.1 \cdot 10^{-6}$ K^{-1} at 0 °C to 1000 °C [2]) and have excellent thermodynamic stability in contact with the surface oxide SiO_2, which grows on such ceramics in usage [1]. State of the art yttria-stabilized zirconia (YSZ) TBCs have excellent thermophysical properties but are limited to operating temperatures below 1200 °C because of a solid-solid phase transition [1,

✉ Julian Gebauer
julian.gebauer@kit.edu

[1] Institute for Applied Materials - Applied Materials Physics, Karlsruhe Institute of Technology, Hermann-von-Helmholtz Platz 1, 76344 Eggenstein-Leopoldshafen, Germany

3]. The temperature limits of $NbAlO_4$ and $TaAlO_4$ seem promising to exceed the limit of YSZ [4–6]. Furthermore, the possible occurrence in refractory metal-alumina composites lead to the investigation of the thermodynamic stability in metal-ceramic composites [5, 7, 8]. Both ternary oxides show no thermodynamic stable phase transition until melting [5]. Metastable phase formation of the tetragonal polymorph of $TaAlO_4$ from the melt and solid-solid transitions of the metastable $TaAlO_4$ polymorphs (tetragonal and orthorhombic) into the thermodynamically stable crystal structure are reported by Feng et al. [6]. Beside the thermal expansion and thermodynamic stability as first selection criteria, more thermophysical properties of the materials in question are needed to estimate the advantages and disadvantages of a new material. Thermal diffusivity and thermal conductivity are the most important properties to describe the heat transfer in a material or manufactured component.

A set of thermophysical data (measurement of thermal diffusivity and the following calculation of thermal conductivity) was published by Chen et al. [1], but calculated with heat capacity obtained by the Kopp-Neumann rule. This work aims to provide a consistent set of experimentally determined data with 2σ uncertainties for thermophysical properties, which are essential for the selection of materials in the development process of new coatings and new use cases in general.

For the system Al–Nb–O, a phase diagram of the quasi-binary section Al_2O_3–Nb_2O_5 was published by Fedorov et al. [4] which was taken as experimental input in the thermodynamic assessment of Gebauer et al. [5]. However, other works give different melting points and in one publication a congruent melting of $NbAlO_4$ is proposed [9–11]. A determination with modern equipment to confirm the invariant temperature published by Fedorov et al. [4] is pending in the literature.

For the system Al–O–Ta, a fusion diagram was published by King et al. [12]. Detailed information could not be obtained, such as the type of reaction of melting (congruent or incongruent) of the ternary oxide $TaAlO_4$. A preliminary assessment by Gebauer et al. [5] used the fusion data of King et al. as congruent melting of $TaAlO_4$. Later, Feng et al. [6] provided a new assessment based on levitation melt experiments with extreme rapid cooling rates. As undercooling is an issue in oxide systems, the determination of the melting with differential thermal analysis (DTA) is still pending in the literature. The congruent melting modeled by Gebauer et al. [5] has been confirmed by Feng et al. [6].

2 Materials and Methods

Materials Mixed oxide powders were used to prepare the samples by solid-state reactions. The used powders are Al_2O_3 TM-DAR from TAIMICRON (99.99 %), Ta_2O_5 puratronic® from Alfa Aesar (99.995 %) and Nb_2O_5 puratronic® from Thermo Fisher (99.995 %). The starting powders were weighted-in in a molar ratio of 1:1 and mixed in dry state in a DAC 150 speedmixer (Hauschild GmbH) for 10 min and then pressed cold-isostatically (in silicone molds, without any binder, wet-bag method) at 500 MPa into pellets. The pellets for the laser flash analysis (LFA) (≈12 mm diameter, ≈2 mm height) were fired for 72 h at 1350 °C ($NbAlO_4$) and 1600 °C ($TaAlO_4$), respectively, in a muffle furnace. Samples for

differential scanning calorimetry (DSC) and DTA were reground and pressed isostatically after the initial synthesis (same as for the LFA samples), and annealed with the same heat treatment again. All samples were analyzed by XRD to verify that they are single phase samples. $NbAlO_4$ and $TaAlO_4$ were determined to be in the thermodynamically stable monoclinic crystal structure $C^2{\cdot}m^{-1}$ (space group # 12) after the initial synthesis as well as after the thermophysical measurements.

Methods For differential thermal analysis, a Setaram SetSys Evolution was used with a high-temperature graphite furnace, tungsten sample holders (type C thermocouple) and tungsten crucibles. The heating and cooling rates were 10 $K{\cdot}min^{-1}$, if not stated otherwise. The shift of crystallization peaks to lower temperatures due to undercooling effects is heavily dependent on the cooling rate, and therefore cooling curves were not evaluated for the determination of melting temperatures. As shown for $TaAlO_4$ in this work, the extrapolated onset temperatures of the peaks in the heating signals are independent of the heating rate. As flowing gas, Argon (99.9999 mass% purity) was used. Due to the lack of calibration possibilities with ITS-90 metals (incompatibility with tungsten crucibles), the correction described below was considered as the most valuable and trustworthy step to correlate the measured temperature close to the real temperature. The sample temperature signal of the DTA was corrected with the following equation: $T_{corr} = T_{exp} + f(T_{exp})$ with T_{corr} being the corrected temperature, T_{exp} being the uncorrected value measured by the DTA, and $f(T_{exp})$ being the linear correction function. $f(T_{exp})$ was determined with the measured melting points of Al_2O_3, Ta_2O_5 and Nb_2O_5 in comparison to literature data [13–15]. All determined melting temperatures were evaluated as extrapolated peak onset temperatures according to Della Gatta et al. [16].

For differential scanning calorimetry, a Netzsch DSC 204 F1 (up to 500 °C, Al crucibles) and a Netzsch DSC 404 F1 (up to 950 °C, Pt crucibles) were used with heating rates of 10 $K{\cdot}min^{-1}$. A τ-sensor (type E thermocouple, Netzsch GmbH) was used in the DSC 204 F1 and was temperature calibrated with several reference materials (adamantane, In, Sn, Bi, Zn, CsCl) provided by Netzsch GmbH. A Netzsch CC300 liquid nitrogen cooling unit was used with the DSC 204 F1 to start measurements at − 20 °C to provide reliable data above 0 °C. The DSC 404 F1 was equipped with a type S sensor, which was operated under argon and argon-oxygen (80:20) gas, but no influence of the atmosphere on the heat flow signals could be detected. The temperature calibration was done using Ag and Au measured under argon (with alumina liner inside the Pt crucibles). The samples were sintered pellets to reach the best possible heat conduction. With polished sample surfaces a good contact between sample and crucible was achieved. Each C_P measurement was done in the three-step method (baseline, reference, sample) according to ASTM E1269-24 [17]. Sapphire standard reference material disks (NIST SRM 720 provided by Netzsch GmbH) were used. All C_P values given in this work are in Joule per Kelvin and per mole of compound. The uncertainties given with the heat capacity data (Eqs. 1 and 2) and in the according plots (Figs. 1b and 3b) are expanded uncertainties with 95 % confidence (coverage factor $k = 2$).

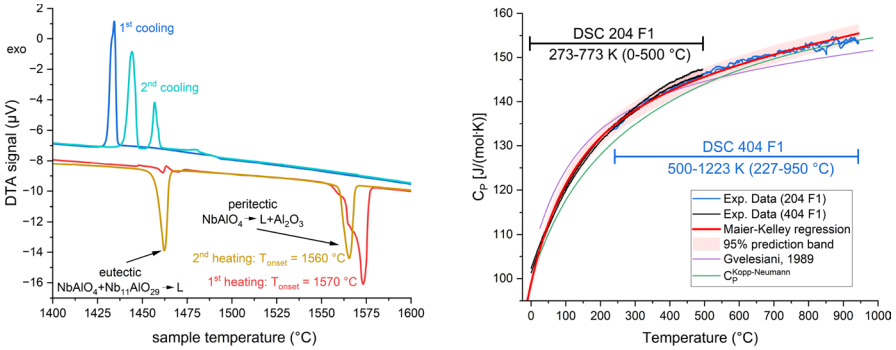

Fig. 1 DTA and DSC results for $NbAlO_4$: (a) DTA signals for the incongruent melting of $NbAlO_4$; (b) experimentally determined heat capacity of $NbAlO_4$ compared to Kopp-Neumann and Gvelesiani et al. [22]

LFA measurements were conducted in a Netzsch LFA 427 from 25 °C up to 700 °C. The samples were coated with carbon spray for good laser pulse absorption. At each temperature step, the thermal diffusivity measurement was repeated at least 5 times with two samples. The measured temperature rise signals were evaluated with the Dusza combined model [18] to obtain the thermal diffusivity data. The density of the LFA samples was determined by the Archimedes method, with pure ethanol. The procedure was repeated with three samples of each phase two times. Both ternary oxides crystallize thermodynamically stable in a monoclinic structure, and therefore have a different thermal diffusivity and thermal conductivity for each crystallographic orientation due to the anisotropy. The used samples are polycrystals derived from fine powders without significant texture after firing, and therefore the samples provide an average over all crystallographic orientations. All values for thermophysical properties derived in this work are such average values.

3 Results and Discussion

3.1 Sample Characterization

$NbAlO_4$ samples had a density of 3.94 ±0.02 g·cm^{-3} and $TaAlO_4$ samples 6.07 ±0.01 g·cm^{-3}, respectively. The porosity was calculated from the measured density and the theoretical density (X-ray density from the unit cell) from Chen et al. [1]. For the $NbAlO_4$ samples, the porosity is 9.4 % and for the $TaAlO_4$ samples 5.5 %, respectively. All samples have less porosity than the maximum recommended value for LFA samples of 10 % according to DIN 18755 [19]. Schlichting et al. [20] analyzed the porosity-dependent thermal conductivity of YSZ (also synthesized from cold-isostatically pressed and sintered powder mixtures) and concluded that the description $\lambda_{dense} = \lambda_{porous} \cdot (1 - 1.5\phi)^{-1}$, following theoretical considerations of Maxwell, fits the experimental findings very well. λ_{dense} is the

thermal conductivity of perfectly dense material, λ_{porous} is the thermal conductivity of the porous sample, and ϕ is the volume fraction of the pores (which is taken as the measured porosity). This correction is also applied in this work and given in the figures for the thermal conductivities.

3.2 $NbAlO_4$

3.2.1 Melting Point

The ternary oxide $NbAlO_4$ melts incongruently: $NbAlO_4 \leftrightarrow liquid + Al_2O_3$ [4]. The invariant temperature was determined by the extrapolated onset temperatures of the DTA heating signals, shown in Fig. 1a. The cooling curves (shifted by +2 μV for better visualization) showed large undercooling effects, which can be explained by the following solidification path: alumina was precipitated from the liquid, then the alumina-depleted liquid was stabilized below the peritectic temperature while precipitation of $NbAlO_4$ occurs and finally the liquid solidified at around the temperature of the eutectic reaction $liquid \leftrightarrow NbAlO_4 + Nb_{11}AlO_{29}$ (1425 °C [4]). In the second heating, the melting of the eutectic can be observed, which is not detected in the first heating's signal. The first heating segment shows a peak with two shoulders (which could be explained by a non-uniform contact between crucible and sample before first melting) and an onset temperature of the main peak of 1570 °C. The second heating signal shows a peak with an onset temperature of 1560 °C. This temperature matches very well with the experimental findings of Fedorov et al. [4].

3.2.2 Heat Capacity

The specific heat capacity of $NbAlO_4$ was determined by using two different DSCs, operated so that the temperature ranges overlapped. Different samples were used for each DSC. The results are plotted in Fig. 1b. The two different DSC experiments show very similar results in the overlapping range, so that a continuous regression with a Maier-Kelley polynomial was done. The polynomial is given in Eq. 1. For comparison, the heat capacity calculated by the Kopp-Neumann rule based on the binary oxide data from NIST [21] is also given in Fig. 1b as well as the data (calculated from enthalpy increment measurements) from Gvelesiani et al. [22]. The measured values show a very similar behavior between 600 °C and 800 °C as the Kopp-Neumann derived data, but show significant deviation outside that range. The previously published data from Gvelesiani et al. lead to a significantly lower heat capacity at high temperatures.

$$C_P^{NbAlO_4}(T/K) = 139.87 \pm 0.04 + (0.01469 \pm 4 \cdot 10^{-5}) \cdot (T/K) + (-3354981 \pm 4098) \cdot (T/K)^{-2} \mathrm{J/(mol \cdot K)} \quad (1)$$

3.2.3 Thermal Diffusivity and Conductivity

The thermal diffusivity data of the LFA measurements are given in Fig. 2a. The thermal diffusivity of $NbAlO_4$ ranges from 0.009 to 0.004 $cm^2 \cdot s^{-1}$. At around 550 °C the thermal diffusivity has a minimum. Above this temperature, the thermal diffusivity increases slightly, in contrast to the expected decrease (which is mainly due to Umklapp-phonon scattering [23, 24]). Caliari et al. [25] detected a similar upwards trend above 400 °C in their thermal diffusivity measurements of Nb_2O_5 coatings. Almadhoni and Khan [26] found a similar trend in several oxides, but at higher temperatures, and stated that the increase is coursed by the increasing influence of radiative transport mechanisms through the sample (infrared radiation) with rising temperatures.

The thermal conductivity of $NbAlO_4$ λ_{NbAlO_4} is shown in Fig. 2b. The error bars indicate the errors propagated from the thermal diffusivity and density measurements. The uncertainty based on the heat capacity measurements are entered as light-red dashed lines: if the upper/lower limit of the 95 % prediction band from the C_P regression polynomial is used for the calculation of the thermal conductivity, the values would be on the light-red dashed lines in Fig. 2b. These lines were added to visualize the uncertainty from the DSC data in comparison to the uncertainty from the LFA measurement. The prediction for perfectly dense $NbAlO_4$ is given as black dashed line, which is calculated using the porosity correction given in Sect. 2. The correction of the experimental data leads to ≈ 16.4 % higher values for perfectly dense material than for the porous samples. λ_{NbAlO_4} is 0.013 to 0.02 $W \cdot cm^{-1} \cdot K^{-1}$, which is at 25 °C an order of magnitude lower than the thermal conductivity of alumina (≈ 0.24 $W \cdot cm^{-1} \cdot K^{-1}$ [27]). $NbAlO_4$ has a similar thermal conductivity as Nb_2O_5 (≈ 0.025 $W \cdot cm^{-1} \cdot K^{-1}$ [25]), but is less thermally conductive than YSZ (0.03 $W \cdot cm^{-1} \cdot K^{-1}$ [20])

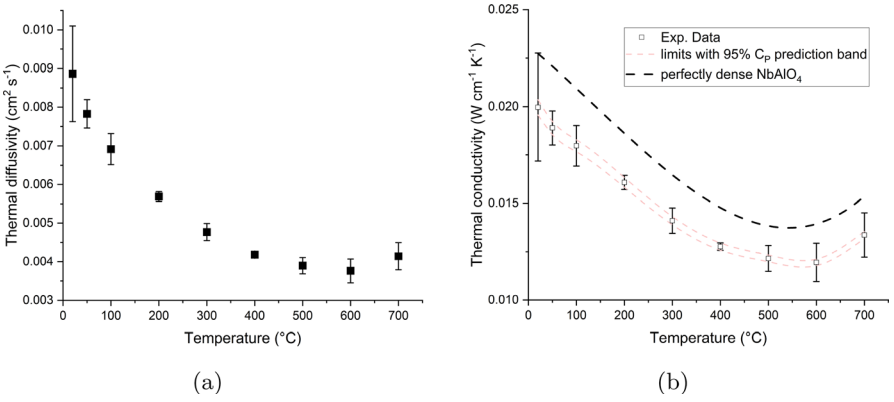

Fig. 2 LFA results for $NbAlO_4$: (a) Thermal diffusivity of $NbAlO_4$; (b) Thermal conductivity of $NbAlO_4$. Boxes: experimentally determined data with light-red dashed limits from the C_P confidence band; black dashed: thermal conductivity of perfectly dense $NbAlO_4$

3.3 $TaAlO_4$

3.3.1 Melting Point

The congruent melting temperature of $TaAlO_4$ was determined with a heating and cooling rate of 5 K·min^{-1} and 10 K·min^{-1} to analyze the undercooling effects. No severe undercooling was observed with 5 K·min^{-1} cooling rate, but undercooling of around 50 K was detected with a cooling rate of 10 K·min^{-1}. As shown in Fig. 3a, the peaks in the heating curves were not shifted between the 5 K·min^{-1} and 10 K·min^{-1} runs. For visualization, the DTA heat flow signals were shifted by +1.5 μV to +10 μV without any influence on the onset temperatures. The onset temperature of the melting peaks is determined to be 1685 °C. This result matches well with the fusion diagram of King et al. [12] (1693 °C) where no indication on the type of reaction is given. The result obtained by Feng et al. [6] (1669 °C) from cooling curves is lower, but the shift to a lower temperature can be explained by undercooling effects also found in this work. In this work, no other peak in the DTA signal was found up to 2000 °C and therefore the melting behavior is determined to be congruent.

3.3.2 Heat Capacity

As for $NbAlO_4$, the heat capacity for $TaAlO_4$ was determined by both DSC machines in two different but partially overlapping temperature ranges. The results show good compatibility between both experiments. To our knowledge, no data have been published so far for the ternary oxide. The Maier-Kelley-type regression lead to a polynomial which represents the temperature range from 0 °C up to 950 °C very well. The polynomial is given in Eq. 2. The heat capacity derived by the Kopp-Neumann rule is leading to much higher values at high temperatures as the experimental

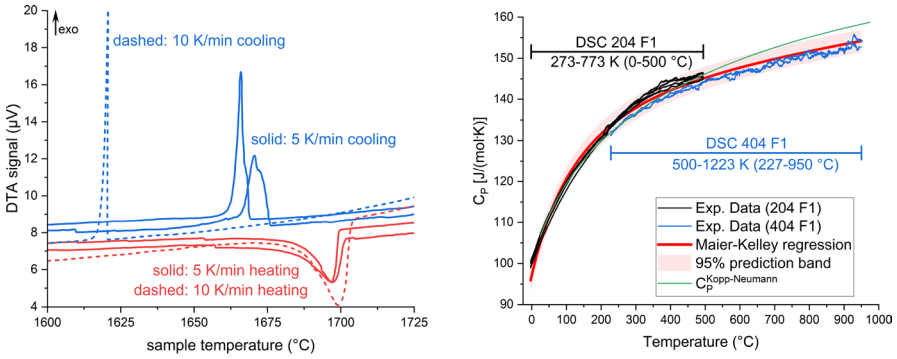

Fig. 3 DTA and DSC results for $TaAlO_4$: (a) DTA signals of the congruent melting of $TaAlO_4$; (b) heat capacity of $TaAlO_4$

results. The Maier-Kelley polynomial gives more reasonable values when extrapolating up to the melting temperature of $TaAlO_4$.

$$C_P^{TaAlO_4}(T/K) = 142.02 \pm 0.04 + (0.01193 \pm 5 \cdot 10^{-5}) \cdot (T/K) + (-3594884 \pm 3114) \cdot (T/K)^{-2} \; J/(mol \cdot K) \tag{2}$$

3.3.3 Thermal Diffusivity and Conductivity

The results of the thermal diffusivity measurements are shown in Fig. 4a. The values for $TaAlO_4$ ranges from 0.017 to 0.005 $cm^2 \cdot s^{-1}$. Compared to $NbAlO_4$, $TaAlO_4$ has a higher thermal diffusivity and no increasing behavior at higher temperatures, which is in accordance with the Umklapp-phonon scattering mechanism [23, 24]. Also, the data obtained by LFA for $TaAlO_4$ have a smaller standard deviation, leading to smaller error bars (compared to Fig. 2a). This can be explained by the smaller porosity of the sample (5.5 % compared to 9.4 % for $NbAlO_4$).

The thermal conductivity of $TaAlO_4$ λ_{TaAlO_4} is shown in Fig. 4b. Uncertainties and influence of the C_P 95 % prediction band are included the same as for $NbAlO_4$ (see Sect. 3.2.3). As the porosity of the sample is only 5.5 %, the correction for perfectly dense $TaAlO_4$ is only $\approx$ 9 % (increase). The thermal conductivity at 25 °C is 0.039 $W \cdot cm^{-1} \cdot K^{-1}$ and approximately by a factor of six lower than that of alumina [27], but slightly higher than that of YSZ (0.03 $W \cdot cm^{-1} \cdot K^{-1}$ [20]).

4 Conclusion

The melting points of the two ternary oxides $NbAlO_4$ (1560 °C) and $TaAlO_4$ (1685 °C) and the fact that no solid-solid phase transition will occur in the oxides are promising results for the possible usage as thermal barrier coatings. Also, the

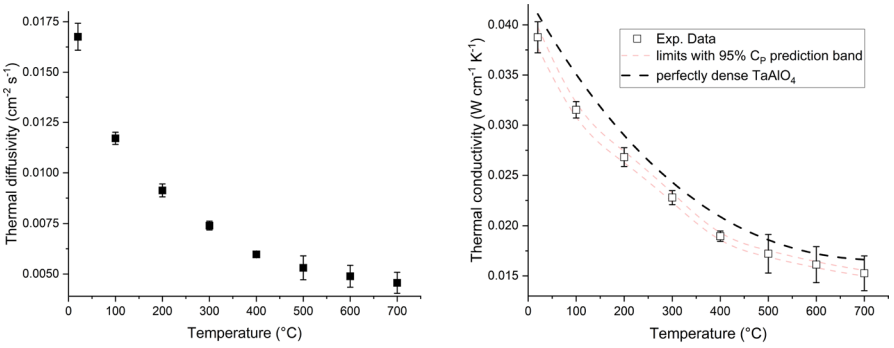

Fig. 4 LFA results for $TaAlO_4$: (a) Thermal diffusivity of $TaAlO_4$; (b) Thermal conductivity of $TaAlO_4$. Boxes: experimentally determined data with light-red dashed limits from the C_P confidence band; black dashed: thermal conductivity of perfectly dense $TaAlO_4$

low thermal diffusivity and thermal conductivity are promising for the usage of both ternary oxides as TBC. The experimental determination of the specific heat is essential, since the Kopp-Neumann prediction deviates more and more from the experimental values with increasing temperature. The given Maier-Kelley polynomials provide a good fit of the experimental data in the measured temperature range and a reliable source for extrapolation of C_P values to high temperatures.

Acknowledgements The authors thank Judith Jung from the Thermophysics and Thermodynamics group at KIT IAM-AWP for preparing samples and conducting experiments.

Author Contributions All authors contributed to the study conception and design. Material preparation, data collection and analysis were performed by Julian Gebauer. The first draft of the manuscript was written by Julian Gebauer, and all authors commented on previous versions of the manuscript. Hans Jürgen Seifert and Peter Franke were responsible for funding acquisition and supervision. All authors read and approved the final manuscript.

Funding Open Access funding enabled and organized by Projekt DEAL. The authors gratefully acknowledge the funding by the German Research Association (DFG) within the Research Groups FOR3010 and FOR3010-2. This work was supported by DFG funding under project number 416817512 with reference numbers FR1108/3-1 and SE647/23-1.

Data Availability No datasets were generated or analysed during the current study.

Declarations

Conflict of interest All authors declare that they have no Conflict of interest.

References

1. L. Chen, M. Hu, J. Feng, Mechanical properties, thermal expansion performance and intrinsic lattice thermal conductivity of $AlMO_4$ (M=Ta, Nb) ceramics for high-temperature applications. Ceram. Int. **45**, 6616–6623 (2019). https://doi.org/10.1016/j.ceramint.2018.12.135
2. Z. Li, R.C. Bradt, Thermal expansion and thermal expansion anisotropy of SiC polytypes. J. Am. Ceram. Soc. **70**, 445–448 (1987). https://doi.org/10.1111/j.1151-2916.1987.tb05673.x
3. M. Zhao, X. Ren, J. Yang, W. Pan, Thermo-mechanical properties of ThO_2 – doped Y_2O_3 stabilized ZrO_2 for thermal barrier coatings. Ceram. Int. **42**, 501–508 (2016). https://doi.org/10.1016/j.ceramint.2015.08.137
4. N.F. Fedorov, I.F. Andreev, R.M. Kasparyan, T.P. Smorodina, Phase equilibria in the Al_2O_3 – Nb_2O_5 system. Izv. Akad. Nauk SSSR. Neorg. Mater. **7**, 643–647 (1971)
5. J. Gebauer, P. Franke, H.J. Seifert, Thermodynamic evaluation of the system Ta–O and preliminary assessment of the systems Al–Nb–O and Al–Ta–O. Adv. Eng. Mater. **24**, 2200162 (2022). https://doi.org/10.1002/adem.202200162

6. Y. Feng, D. Zhao, Z. Pi, D. Huang, F. Zhang, Phase equilibrium investigations of the $Al_2O_3 - Ta_2O_5$ system: new experiments and thermodynamic modeling. J. Am. Ceram. Soc. **107**, 6939–6954 (2024). https://doi.org/10.1111/jace.19957
7. A. Weidner, Y. Ranglack-Klemm, T. Zienert, C.G. Aneziris, H. Biermann, Mechanical high-temperature properties and damage behavior of coarse-grained alumina refractory metal Composites. Materials **12**, 3927 (2019). https://doi.org/10.3390/ma12233927
8. M.K. Eusterholz, T. Boll, J. Gebauer, A. Weidner, A. Kauffmann, P. Franke, H.J. Seifert, H. Biermann, C.G. Aneziris, M. Heilmaier, High-temperature ternary oxide phases in tantalum/niobium–alumina composite materials. Adv. Eng. Mater. **24**, 2200161 (2022). https://doi.org/10.1002/adem.202200161
9. G. Layden, The system $Al_2O_3 - Nb_2O_5$. J. Am. Ceram. Soc. **46**, 506–506 (1963)
10. E.N. Isuprova, N.A. Godina, E.K. Keler, Reactions in the systems $Al_2O_3 - Nb_2O_5$ and $Al_2O_3 - Ta_2O_5$. Neorg. Mater. **6**, 1465–1469 (1970)
11. A. Burdese, M. Lucco-Borlera, P. Rolando, Sistemi tra anidride niobica ed ossidi di alluminio e cromo. Atti Acca. Sci. Torino, Cl. Sci. Fis., Mat. Nat. **99**, 1079 (1964/1965)
12. B.W. King, J. Schultz, E.A. Durbin, W.H. Duckworth, Some properties of tantala systems. https://www.osti.gov/biblio/4352714
13. S. Schneider, Cooperative determination of the melting point of alumina. Pure Appl. Chem. **21**, 115–122 (1970). https://doi.org/10.1351/pac197021010115
14. S.P. Garg, N. Krishnamurthy, A. Awasthi, M. Venkatraman, The O–Ta (Oxygen–Tantalum) system. J. Phase Equilib. **17**, 63–77 (1996). https://doi.org/10.1007/BF02648373
15. R.P. Elliott, Columbium-oxygen system. Trans. Am. Soc. Met. **52**, 1 (1960)
16. G. Della Gatta, M.J. Richardson, S.M. Sarge, S. Stølen, Standards, calibration, and guidelines in microcalorimetry. Part 2. Calibration standards for differential scanning calorimetry*(IUPAC Technical Report). Pure Appl. Chem. **78**, 1455–1476 (2006). https://doi.org/10.1351/pac200678071455
17. ASTM E1269-24, Standard Test Method for Determining Specific Heat Capacity by Differential Scanning Calorimetry, 2024
18. L. Dusza, Combined solution of the simultaneous heat loss and finite pulse corrections with the laser flash method. High Temp. High Press. **27**, 467–473 (1995)
19. DIN EN ISO 18755:2023, Hochleistungskeramik-Bestimmung der Temperaturleitfähigkeit monolithischer Keramik mit dem Flash-Verfahren
20. K. Schlichting, N. Padture, P. Klemens, Thermal conductivity of dense and porous yttria-stabilized zirconia. J. Mater. Sci. **36**, 3003–3010 (2001). https://doi.org/10.1023/A:1017970924312
21. M.W. Chase, NIST-JANAF thermochemical tables 4h ed. J. Phys. Chem. Ref. Data **9**, 1–1951 (1998)
22. G.G. Gvelesiani, I.S. Omiadze, A. Nadiradze, High-temperature enthalpy and heat capacity of aluminum and yttrium niobates. Inorg. Mater. **25**, 1757–1759 (1989)
23. R. Peierls, Zur kinetischen Theorie der WÃ¤rmeleitung in Kristallen. Ann. Phys. **395**, 1055–1101 (1929). https://doi.org/10.1002/andp.19293950803
24. T.M. Tritt, Thermal conductivity: theory, properties, and applications, in *Physics of solids and liquids*. (Kluwer Academic/Plenum Publ, New York, 2004)
25. F.R. Caliari, E. Garcia, F. Miranda, G.P. Filho, S. Sampath, Phase evolution in plasma sprayed Nb_2O_5 coatings. J. Eur. Ceram. Soc. **41**, 5248–5257 (2021). https://doi.org/10.1016/j.jeurceramsoc.2021.04.022
26. K. Almadhoni, S. Khan, Evaluation of the effective thermal properties and aluminum metal matrix composites reinforced by ceramic particles. Int. J. Current Eng. Techn. **5**, 2884–2897 (2015)
27. J. Hemrick, J.C.W. Kistler, A. Wereszczak, M. Ferber, Thermal conductivity of alumina measured with three techniques. J. Test. Eval. **31**, 438–442 (2003). https://doi.org/10.1520/JTE12368J